Acta Acustica 2024, **8**, 56

https://doi.org/10.1051/aacus/2024052

Available online at:
https://acta-acustica.edpsciences.org

Topical Issue - Active Noise and Vibration Control

SCIENTIFIC ARTICLE OPEN ACCESS

# Towards an active semi-anechoic room: simulations and first measurements

Cédric Pinhède[1,*], Romain Boulandet[2], Emmanuel Friot[1], Mark R. Allado[2], Renaud Côté[1], and Philippe Herzog[3]

[1] Aix Marseille Univ, CNRS, Centrale Med, LMA, 4 impasse Nikola Tesla, 13013 Marseille, France
[2] University of Applied Sciences and Arts Western Switzerland, 4 rue de la Prairie, 1202 Geneva, Switzerland
[3] ARTEAC-LAB, 29 Rue Saint-Savournin, 13005 Marseille, France

Received 27 February 2024, Accepted 13 August 2024

**Abstract** – Semi-anechoic rooms are used for the acoustic characterisation of noise sources. They involve heavy infrastructures and thick absorbent lining. The aim of this work is to demonstrate a less expensive alternative by complementing a thin passive coating with an active technology. Previous work has achieved the active reduction of the pressure scattered by the reflective wall of a semi-anechoic room, in the 80–200 Hz frequency band. This work validated an innovative approach allowing to control the scattered pressure throughout the measurement volume, using a setup located over its periphery. This paper extends a previous presentation at Forum Acusticum dealing with the active control of the low-frequency reflections on the walls and ceiling of a semi-anechoic room [Pinhède et al., Forum Acusticum 2023, Torino, Italy, 11–15 September, 2023, https://doi.org/10.61782/fa.2023.0399]. We describe the design principles and the 2D semi-analytical and 3D finite element simulations of the control system that help optimise parameters such as the transducers number and locations. A full-scale demonstrator has been built to validate the control strategy. Acoustics measurements, which have been used to characterise the room acoustics and to update the simulation parameters are also presented and compared to an updated numerical model.

**Keywords:** Semi-anechoic room, Active noise control, Acoustical measurement, Active anechoicity

## 1 Introduction

Current standards for the measurement of loudspeaker drivers or systems require so-called "free field" measurement conditions, i.e. measurements performed in anechoic or semi-anechoic rooms [1]. A few standards for determining the sound power level of noise sources also require such facilities [2]. To approximate free-field conditions, suitable facilities involve a large room with a thick lining over the absorbing walls. Whatever the absorbing material involved, such a facility cannot be anechoic at very low frequencies: it is restricted to frequencies above its so-called "cut-off frequency", mainly determined by the lining thickness.

Alternatives have been proposed to avoid the cost and burden of building the large measurement facilities which would be needed for measurements below 100 Hz: sound power levels may be estimated using acoustic intensity measurements [3, 4], and loudspeaker responses may be performed using near-field and gated measurements [5]. More elaborate methods even aim at estimating the anechoic 3D radiated field by using a set of pressure measurements and sound field models allowing to extrapolate the measurements [6–8].

Although such estimation methods may be quite sufficient in some cases, they rely on assumptions which may not be satisfied in complex or specific radiation situations and cannot avoid physical phenomenon related to the interaction between the studied source and the surrounding walls (acoustic loading, higher order diffraction, etc). Especially, for laboratory use, actual anechoic rooms are still preferred – but even the larger ones barely allow to measure a source at frequencies lower than 60–70 Hz.

This motivated initial work trying to design a low-frequency anechoic room by using the complementarity between absorbing material and active control techniques, which have their best performances at lower frequencies [9, 10]. This should allow to design hybrid solutions combining a thin absorbing layer with a set of control sources driven by a controller which tries to minimise an error quantity.

Such active control of scattered acoustic fields has already been studied, mainly to deal with the field scattered by bodies in water [11] or air [12]. Many authors have since proposed strategies to deal with scattering control or acoustic cloaking, however mostly through simulations [13–17].

*Corresponding author: pinhede@lma.cnrs-mrs.fr

Indeed, the practical design of an active anechoic room requires to be able to minimise the acoustic field scattered by the room walls, which is not physically different from the direct field and cannot thus be directly measured; some kind of virtual sensing is thus required. It has been shown that, close to the walls, a single linear operator links the total acoustic field to the field scattered by these walls, whatever the direct acoustic field [18]. A preliminary identification may then allow to estimate experimentally this operator. When possible, this identification may be performed by removing the scattering object – but it is not possible to remove the room walls.

Practical implementation of active anechoicity has thus been the topic of a long-term research program at LMA. It started by theoretical work and experiments on the mock-up of an anechoic room [19–21], followed by a first full-size experiment of acoustic cloaking of the reflective wall of a semi-anechoic room in the 80–200 Hz frequency band [22, 23]. Although the ultimate goal is to build active scattering control in a large anechoic room at LMA, an intermediate project has been targeted in 2021: it deals with a small semi-anechoic room usable by Small and Medium-sized Enterprises' (SME) at design stage. The project described thereafter, named "DADA" (french acronym for "anti-diffractive acoustic dome"), thus aims at dealing with five walls covered by a thin passive liner combined with active scattering control. The resulting facility should be a semi-anechoic room of relatively small footprint (targeted dimensions $W = 4.5$ m; $D = 3.65$ m; $H = 3$ m are compatible with usual buildings) but able to deal with the whole frequency range of standard measurements. It is depicted by Figure 1.

The present paper was written upon a suggestion to extend a presentation at the 2023 edition of Forum Acusticum [24]. Sections 2–4 are therefore taken from this presentation, with some improvements and more details: Section 2 recalls the strategy developed for the global active control of reflections on the walls of a room. Sections 3 and 4 respectively deal with improved 2D and 3D numerical simulations of the targeted demonstrator. Section 5 presents the experimental setup which has been built at LMA; first measurements are then compared to new Finite Element Modelling (FEM) simulations, after careful tuning of model parameters to match the experimental conditions [25]. Section 6 then concludes the paper.

## 2 A strategy for global active control of low-frequency wall reflections in a semi-anechoic room

A strategy was proposed a few years ago for estimating the acoustic pressure scattered by a surface from measurements of the total pressure in front of that surface [12, 18, 23]. This strategy makes it possible to envisage the setup illustrated in Figure 1 for the active control of undesirable reflections occurring at low frequencies on the walls and ceiling of a semi-anechoic room: control sources are placed on the walls and ceiling of a semi-anechoic room to minimise the acoustic field scattered on a set of

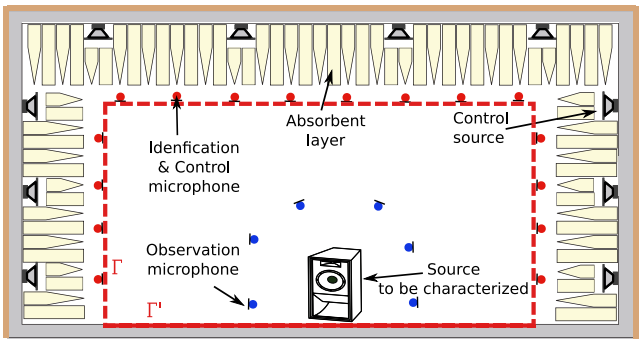


**Figure 1.** Principle of a semi-anechoic room with active technology.

microphones meshing a surface $\Gamma$ close to the walls to be treated. Since $\Gamma$, completed by its symmetric with respect to the floor, is a closed surface, cancelling the pressure scattered by the walls on $\Gamma$ means that it is cancelled over the entire interior volume of the room, except in theory at certain Dirichlet resonance frequencies [26]. As all the transducers required for active control are located on or close to the walls, measurements with observation microphones around the source to be studied can be carried out as in an ordinary room without active control.

We show below how the pressure scattered on each of the microphones $\Gamma$, in the presence of an unknown source placed in the room, can be estimated by linear filtering of the total pressure measured on all these microphones. Once the set of minimisation signals accounting for the scattered field can be computed, open-loop or adaptive (e.g. FxLMS) control can be implemented as usual with minimisation microphones.

### 2.1 The scattered pressure as linear filtering of total pressure measurements

If $G$ denotes *the* Green's function for the Helmholtz equation of the semi-anechoic room *without walls and ceiling* ($G$ is the free half-space Green function if the floor $\Gamma'$ is perfectly plane and acoustically rigid), the Green's representation of the total pressure at any point in the room can be written at pulsation $\omega$, whatever the source present (see e.g. [27], p. 321):

$$p_{\text{total}}(\mathbf{r},\omega) = p_{\text{direct}} + p_{\text{scattered}} = p_{\text{direct}} + \int_{\Gamma}\left[G(\mathbf{r}|\mathbf{r}_0,\omega)\frac{\partial}{\partial n_0}p(\mathbf{r}_0,\omega) - p(\mathbf{r}_0,\omega)\frac{\partial}{\partial n_0}G(\mathbf{r}|\mathbf{r}_0,\omega)\right]d\Gamma_0. \quad (1)$$

The scattered pressure due to the walls is an integral of the pressure and normal pressure gradient over $\Gamma$ with weights which do not depend on the acoustic sources. It can therefore theoretically be calculated from pressure field measurements over $\Gamma$ without any knowledge of the acoustic sources involved.

The integral in equation (1) could indeed be calculated from discrete measurements over $\Gamma$, provided that a

sufficient number of pressure and pressure gradient measurements are taken on the surface and that the floor allows the use of the Green's function of the free half-space. In practice, however, pressure gradient measurements are difficult to achieve at low frequencies, and require much more expensive sensors than ordinary low-cost microphones. This is why in previous work we conjectured that the scattered pressure could be expressed as an integral over the pressure alone. This is notably the case if $\Gamma$ behaves as a locally reacting surface with a specific admittance $\beta$, in which case the pressure gradient in equation (1) can be replaced by a pressure-dependent term:

$$\frac{\partial}{\partial n_0} p(\mathbf{r}_0, \omega) = -jk\beta p(\mathbf{r}_0, \omega). \tag{2}$$

In the general case, it is difficult to determine under which theoretical conditions the scattered pressure can be expressed as an integral over pressure alone [18], but in all the cases studied, and in particular in the simulations presented below, measurements of pressure alone allowed a very accurate computation of the scattered pressure. Discretisation of the pressure integral, with more than two sensors per wavelength, finally allows to express the scattered pressure as a function of discrete pressure measurements over $\Gamma$:

$$p_{\text{sca}}(\mathbf{r}, \omega) \approx \sum_k g_k(\mathbf{r}, \omega) p_k(\mathbf{r}_k, \omega). \tag{3}$$

The scattered pressure at any location in the room can therefore be estimated through linear filtering of total pressure measurements over the room walls and ceiling.

### 2.2 Identification of the scattering filters

The scattering filters $g_k(\mathbf{r})$ in equation (3) result from a complex combination of Green's function, equivalent surface impedances and surface discretisation weights. Furthermore if cheap, non-calibratable microphones are used, the acoustic pressure required in equation (3) cannot be accurately derived from the measurement signals. The scattering filters, however, do not depend on the acoustic sources. A procedure has therefore been developed and validated in a semi-anechoic room to determine the filters to be applied to pressure signals in order to accurately estimate the pressure scattered by a given surface, see [23]: a reference source, with a known free-field radiation pattern, is placed at several points in the semi-anechoic room. Assuming that the ground is rigid, the source's direct pressure in the free half-space can be calculated and substracted from the total pressure measurements to generate scattered pressure signals. By solving an inverse problem, we then identify off-line scattering filters that match total pressure measurements to scattered pressure.

### 2.3 Control of the scattered pressure

As stated above, once the set of minimisation signals accounting for the scattered field are computed, usual control algorithms can be implemented for minimisation. The control strategy [23] consists of minimising the scattered pressure close to the walls in order to obtain its cancellation inside the volume. The transfer matrix $\mathbf{H}$ is computed between the secondary sources and the pressure at the minimisation points At each frequency, the control vector $\mathbf{u}$, to be supplied to the secondary sources for control, must minimise the criterion:

$$J = ||\mathbf{p}_{\text{sca}} + \mathbf{H}\mathbf{u}||^2. \tag{4}$$

## 3 2D numerical simulations

The initial simulation results of the device were carried out using a semi-analytical model of a 2D room with low-absorbing walls. 2D representations make it easier than 3D to visualize the number of transducers per wavelength required for effective active control. A model that requires very little computing time also makes it easy to optimise the number and position of transducers. Although the walls and ceilings of semi-anechoic rooms are absorbent, the focus here is on very low-frequency reflections for which absorption is low, and we wish to compare the calculations with experimental measurements in a room initially devoid of absorbers, which justifies the use of the model presented below.

### 3.1 The room acoustic model

To a first approximation, the low-frequency acoustics of a cavity with low-absorbing walls can be described using a series of rigid cavity modes $\psi_n$ with associated modal damping ratios $\xi_n$, see e.g. [27], p. 554. The transfer function between a monopole source with flow rate $q$ at location $\mathrm{r}_0$ and the acoustic pressure at location r can then be written at angular frequency $\omega$ as:

$$p(\boldsymbol{r}, \mathbf{r}_0) = \rho c^2 j\omega q \sum_{n=0}^{+\infty} \frac{\boldsymbol{\psi}_n^t(\mathbf{r})\boldsymbol{\psi}_n(\mathbf{r}_0)}{(\omega_n^2 + 2j\xi_n\omega_n\omega - \omega^2)\int_V \boldsymbol{\psi}_n^2 \mathrm{d}V} \tag{5}$$

where $c$ is the sound speed. In a 3D parallelepided or 2D rectangular cavity, the rigid eigenmodes are the usual products of cosine functions of the space variables. The damping ratios can be taken as the damping ratios from the complex mode resulting from the FEM of the room including wall absoption.

A 4.5 m × 3.65 m × 3 m room with an inner plasterboard layer has been built at LMA to house and test the DADA. In order to compute damping ratios, 2D and 3D FEM has been implemented for a room with these dimensions and with real-valued wall and ceiling impedance accounting for a 2% absorption at low frequency.

The 2D simulations below take the 83 modes with a resonance frequency below 500 Hz into account. The first mode damping ratios are worth about 0.4% and decrease when frequency increases. Modes involving a pressure maximum on two walls appear to be more damped than modes with maxima on the floor and ceiling, which seems logical.

### 3.2 Source model and optimal control

In the simulations below, all the acoustic sources are considered as monopoles. This makes control perform worse because the radiating from a real wall-mounted control source will be closer to the frontwave scattering from the walls than the one from a theoretical monopole. The acoustic field near the walls with monopoles is more complex than with extended sources, global control is therefore more difficult to obtain from control at sensors close to the walls because of near-field effects. In the simulations below optimal control is derived in the frequency domain through matrix pseudo-inversion at each frequency, which leads to better results than could be achieved with real-time control of the scattered pressure in the case of a wide band primary source. The scattering filters are also derived by pseudo-inversion of the acoustic data generated by the reference source.

### 3.3 2D simulation results

Figure 2 shows one of the 2D configurations studied: 11 wall-mounted control sources are used to cancel out the scattered pressure at 18 microphones close to the walls (in front of the absorber wedges in a real room).

The scattered pressure at each microphone is estimated by linear filtering of the total pressure at all microphones. The linear filters are calculated by solving an inverse problem generated by moving a reference source, whose free-field radiation pattern is known, to 12 locations meshing one-ninth of the room surface. Figure 3 presents the singular values of matrix whose pseudo-inversion gives the scattering filters. The matrix condition number is fearly reasonable and do not require a complex regularization scheme.

Slightly irregular microphone positions have been chosen, in order to avoid the singular frequencies that may appear when implementing active control on a closed surface: the cancellation of pressure on a regular surface does not guarantee its cancellation inside the encolsed volume at the resonance frequencies of the associated Dirichlet problem [26]. Three hundred and fifty two additional measurements points meshing one center quarter of the room were considered to assess the control performance in the measurement zone of interest.

The curves of Figure 4 correspond to the ratio (expressed in dB) between the total pressure with and without control and the direct pressure computed in free half-space. The 0 dB value should thus correspond to a semi-anechoic situation and deviations from 0 dB illustrate the effect of the actual boundary conditions. The horizontal dashed lines at ±2.5 dB represent the admissible deviations from the theoretical decay (inverse square law) according to ISO 3745 standard [2].

The results presented are calculated from the Root-Mean-Square (RMS) value over 352 assessment points when a primary source with flow rate $q_0 = 10^{-4}$ m$^2$/s is placed at the center of the room floor. The total primary pressure has large fluctuations, following the room resonances, instead of the smooth pressure response expected in free half-space. Scattering control leads to a large reduction of these undesirable fluctuations, both when the exact scattered pressure or the estimated one from total pressure measurements is minimised on microphones close to walls. Notably, the results obtained with scattering control are within the admissible deviations up to 350 Hz.

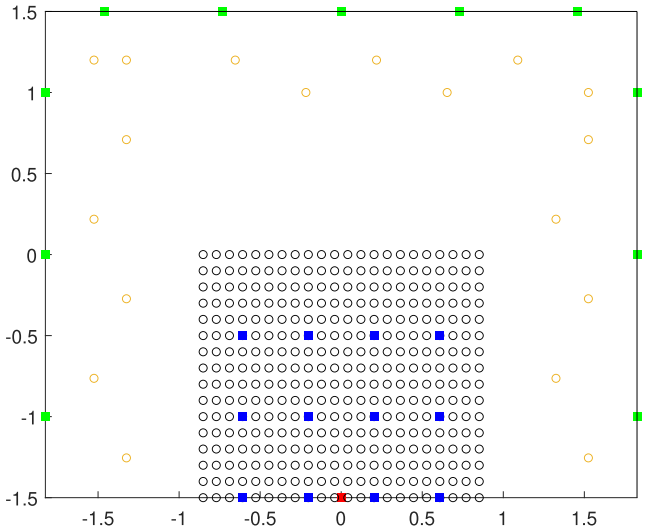


**Figure 2.** The DADA 2D simulation setup: monopole primary source ■, control sources ■, reference source locations ■, total pressure measurement and scattered pressure minimisation points ○, assessment points ○.

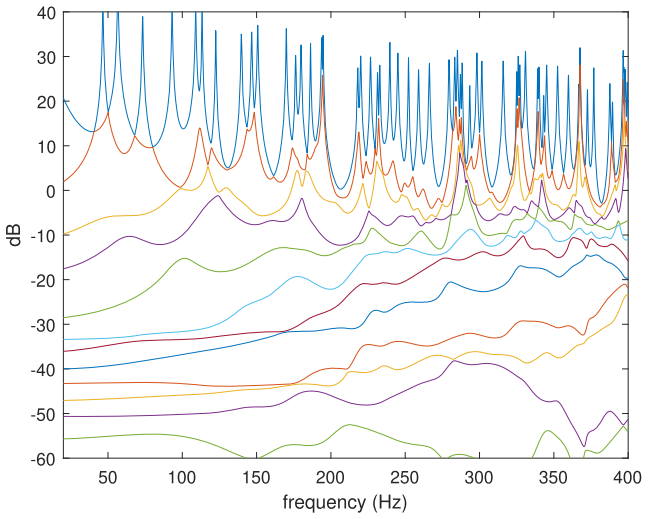


**Figure 3.** Singular values of the matrix used to estimate the scattered pressure.

The 2D simulations presented in this section helped to validate the principle of identifying scattering filters. They also showed that the control of the scattered field in the vicinity of the walls leads to control the scattered field in the measurement zone at the centre of the semi-anechoic room. Such 2D simulations also make it possible to quickly test the effect of changes in the general organisation of the control setup and provide information on the density of

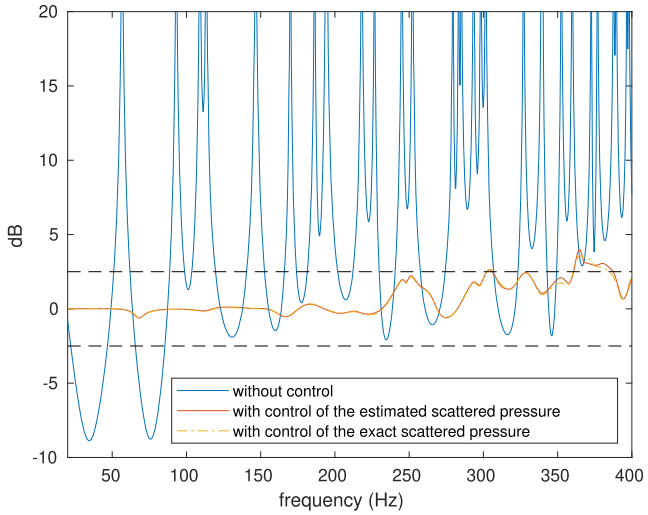


**Figure 4.** RMS at the 352 assessment points of the total pressure normalized by the direct pressure.

transducers to be used as a function of frequency for global control. However, full 3D calculations, taking into account the frequency-dependent wall absorption and the finite size of the sources, are needed to determine the experimental setup to be effectively tested in practice. Such 3D simulations were therefore carried out using a FEM model and are presented below.

## 4 3D numerical simulations

The following 3D simulations are performed using COMSOL Multiphysics® 5.6 and connected to MATLAB® control simulations through the LiveLink for MATLAB® extension. This software combination allows a great flexibility for the simulation of the different steps involved in scattering control, at the price of somewhat long computation times – it is thus not convenient for parametric studies, most of which were conducted using the 2D semi-analytical model.

### 4.1 Simulated configuration

The targeted room is modelled as a rectangular block of dimension $4.5 \times 3.65 \times 3$ m$^3$. An impedance condition of $8.10^4$ Pa.s/m is applied to all walls. The floor is modelled as an acoustically hard boundary. The mesh is controlled by the physics of the model taking into account the maximum wavelength of the simulation. The simulations are performed over 20–200 Hz frequency range in 1 Hz steps. The computation time required to solve the model, which includes 32,000 domain elements, is around 1500 s on a desktop computer for 181 frequency steps.

Figure 5a shows the modelled room and the positions of the 62 minimisation points uniformly distributed over a closed surface surrounding the control volume. Before simulating scattering control, a preliminary identification phase requires the calculation of all transfer function between the minimisation points and the identification sources located in the control volume shown in Figure 5b.

### 4.2 Preliminary identification of the scattering filter

This preliminary step is needed in order to estimate the operator linking the total and scattered pressures at the minimisation microphone locations. For this estimation, identification sources distributed in the measurement volume are modelled as monopoles with flow rate $q_0 = 10^{-4}$ m$^3$/s.

Direct pressures $p_{\text{dir}}$ are then computed at each identification microphone (MicID) position, by considering the radiation of the monopole in a half-space closed by a Perfectly-Matched Layer (PML), see Figure 6. The total pressures $p_{\text{tot}}$ are calculated the same way but in the rectangular room with boundary specific impedance condition of $198\rho c$ which leads to 2% absorption applied to all walls, see Figure 7.

Both computations ($p_{\text{dir}}$ in free half-space and $p_{\text{tot}}$ in the room) are done iteratively for each identification source (SourceID), with identification positions identical to the minimisation positions. This allows to deduce the exact scattered pressures $p_{\text{sca}} = p_{\text{tot}} - p_{\text{dir}}$ at the minimisation positions.

A matrix relation may thus be defined between the scattered pressure $p_{\text{sca}}$ and the (measured) total pressure $p_{\text{tot}}$ at the minimisation points. The identification of this so-called "scattering filter" is obtained by solving the inverse problem using the data set of scattered and total pressures generated with the 72 identification sources, see details in [23]. This inverse problem is over-determined and thus do not require any significant regularization.

### 4.3 Control configuration and results

Scattering control may then be simulated, by minimising the scattered pressure $p_{\text{sca}}$ at the 62 positions, located close to the walls, used to estimate the scattering filter. This microphone number results from 2D simulations, which also lead to use 54 control sources distributed over the 5 walls (except the floor). The frequency response functions (FRF) between the control sources and all the microphones are then computed by applying successively to each source an acceleration $a = j\omega q_0/S$ where $S = 0.0133$ m$^2$ is the surface area of each piston.

When the responses of all control sources and of the primary source (to be measured) have been estimated, optimal control may be computed in order to minimise the estimated scattered pressure on the microphone set used previously for the identification of the scattering filter: At each frequency, the $\mathbf{u}$ commands obtained from equation (4) are supplied to the control sources modelled as plane pistons positioned over the walls of the room, see Figure 8.

Thanks to the 3D FEM model, individual responses of the primary and control sources may be combined with the weighting computed for optimal scattering control, allowing to visualise the resulting pressure everywhere inside the room and over its walls.

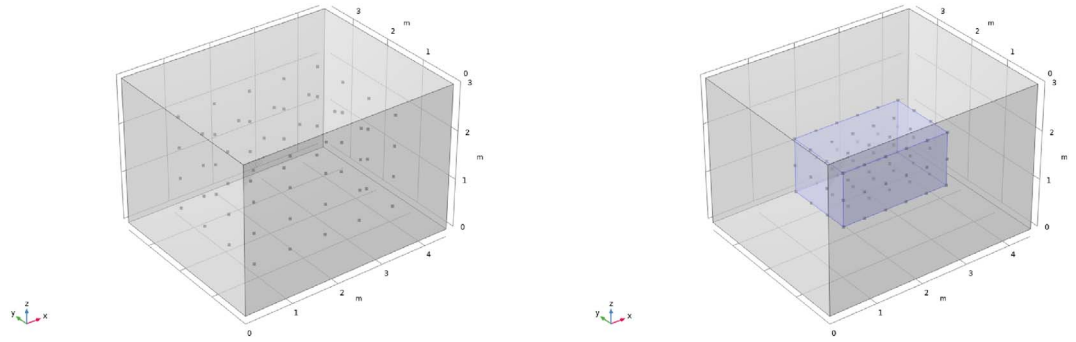

(a) (b)

**Figure 5.** The 3D simulation setup, (a) Location of the 62 minimisation points, (b) Location of the 72 identification sources.

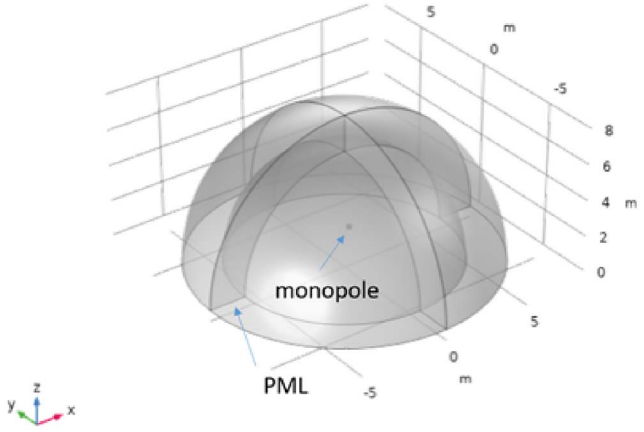


**Figure 6.** Radiation of a monopole in a half-space.

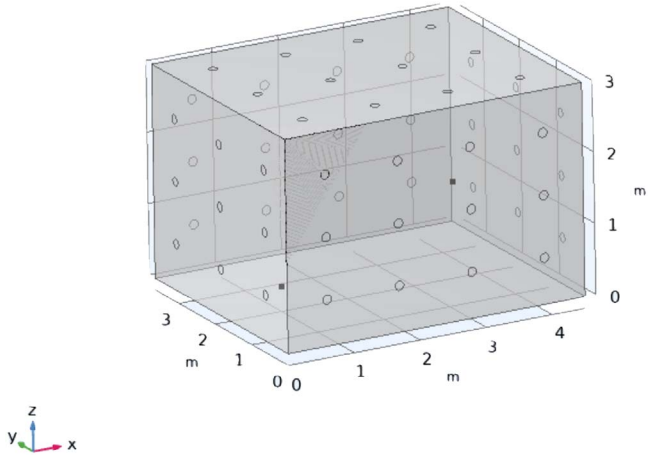

**Figure 8.** Positions of control sources.

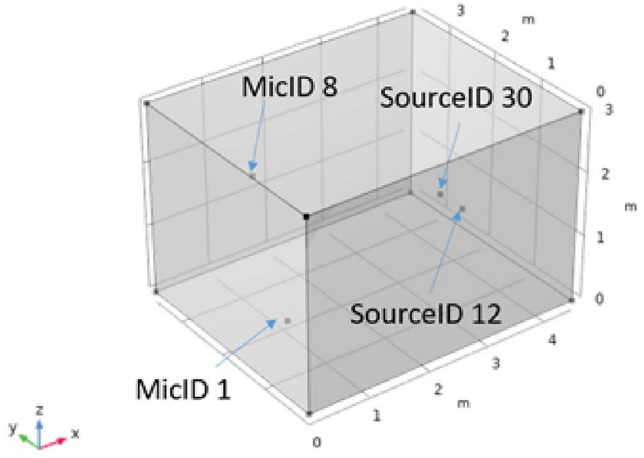


**Figure 7.** Source (number 12, 30) and microphone (number 1, 8) identification positions.

#### 4.3.1 Local pressures

As a first illustration, we present curves for an identification microphone and a primary source. Two cases are shown: the first one involves primary source SourceID 12 and pressure on microphone MicD 1; the second case involves primary source SourceID 30 and microphone MicD 8. Figure 9 shows the pressure levels between 20 Hz and 200 Hz with and without control for these two examples.

Figure 9 shows pressures estimated with control minimising either the exact (label "$P_{\text{on}}$ exact") or the estimated (label "$P_{\text{on}}$ estimated") scattered pressure. Among the curves, $P_{\text{dir}}$ corresponds to the radiation from the primary source in a half-space closed by a PML and $P_{\text{tot}}$ and $P_{\text{scat}}$ correspond to the radiations from the primary source in the room with specific impedance conditions at the boundaries (cf. Sect. 4.2).

Without surprise, the total pressure $P_{\text{tot}}$ is dominated by the modal behaviour of the room, showing peaks and dips corresponding respectively to the pressure resonances and nodes at the observation point. Note that the total pressure field is dominated by the scattered pressure field. Conversely, the controlled pressure is close to the direct pressure with attenuations up to 30 dB around certain room modes.

In addition, the identification of the scattering filter from simulated results is quite correct: the control results using either the exact or the estimated scattered pressure are almost equivalent. The simulated control is effective

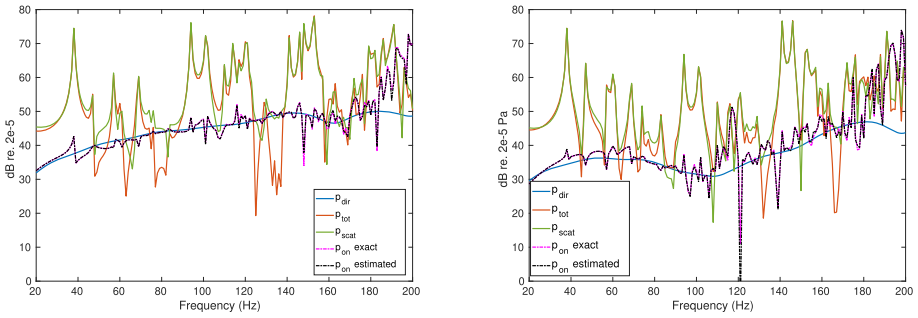


(a) (b)

**Figure 9.** Sound pressure level with and without control (a) on microphone MicD 1 for the primary source SourceID 30, (b) on microphone MicD 8 for the primary source SourceID 12.

up to 180 Hz. Figure 9b however shows a specific situation for which the results of the control exhibits a very marked dip around 120 Hz. The loss of controllability at this frequency could be due to the particular arrangement of the transducers. This may be an irregular frequency at which control of the pressure at surface mapped by microphones does not allow full control inside the surface. This issue is currently under investigation.

#### 4.3.2 Pressures on the walls

The 3D model also allows to display pressure maps on the room walls, illustrating the effect of control sources. The case studied here is identical to the previous one for primary source SourceID 30, located at position $X = 2.4$ m, $Y = 1.58$ m, $Z = 1.35$ m. For this second set of simulations, only the exact scattered pressure is used when computing control commands. Results are presented at a few frequencies: 38 Hz, 69 Hz, 101 Hz, 120 Hz, 125 Hz, 186 Hz. High pressures are shown in red and pressure nodes in blue.

Figure 10 shows the total pressure distribution over the room walls, without control. The expected modal shape for the room modes are (1, 0, 0), (1, 0, 1), (1, 0, 2), and (1, 3, 2) respectively at frequencies 38 Hz, 69 Hz, 101 Hz, 120 Hz, 186 Hz. These modes correspond to peaks seen in Figure 9a. At 125 Hz, the total pressure distribution does not correspond to a modal shape see Figure 10e and is located in a pressure node see Figure 9a.

Figure 11 shows the same pressure distributions with scattering control: the pressure distribution is significantly altered and the room's natural modes are no longer distinguishable. The average pressure level is significantly reduced on the walls, especially on the floor, except at 186 Hz where it is higher on all walls, see Figure 11f: this frequency seems to high to be controlled with the setup considered here.

When scattering control is effective, the pressure is reduced in average over the walls, but it is quite high in the vicinity of the control sources, where their nearfield dominates the room modes. This shows that minimisation microphones should not be placed close to the control sources, otherwise a bias would result from this near-field pressure.

Examining the distribution of commands delivered to the control sources show that they depend on the shape of the mode to be attenuated. The amplitude of the control source levels also varies with frequency, and these levels are very high at 69 Hz and 186 Hz. The regular placement of the control sources might not allow specific modes to be controlled efficiently.

#### 4.3.3 Pressure inside the room

Figure 12 presents slice plots showing how pressure is distributed inside the room with scattering control, for the same configuration as in the previous section. Surfaces are in the $XZ$ and $YZ$ planes of the primary source, the position of which appears as a red spot near the center of the slice. The total sound pressure tends towards the free field response of the primary source in a large volume around it. Conversely, high pressure levels are seen close to the walls, because of the near-field radiation of control sources.

These maps also show how the commands applied to the control sources depends on the shape of the room modes to be controlled. Especially, control of the scattered pressure at frequencies 69 Hz, 101 Hz and 186 Hz (Figs. 12b, 12c, and 12f) lead to high amplitudes of the control sources. However the control performances are different for these three frequencies: scattered pressure is significantly minimised at 69 Hz but less at 101 Hz, while at 186 Hz the control diverges. The symmetrical arrangement of the control sources could again explain the lack of efficiency for controlling this mode shape: the control sources are located on the pressure nodes at 101 Hz, see Figure 10c. At 186 Hz, the modal structure is more complex, and the small number of control sources and their non-optimised positions seem to be insufficient for effective control.

Globally, the above results show that the simulated control is quite satisfactory up to 120 Hz, and still interesting up to 180 Hz. These results also demonstrate that controlling the scattered pressure close to the walls results in its cancellation inside the volume of the room.

The 3D modelling developed for the room allows us to observe the behaviour of the control sources on the wall and the extension of the controlled zone inside the volume of the room. It also shows how the contribution of the

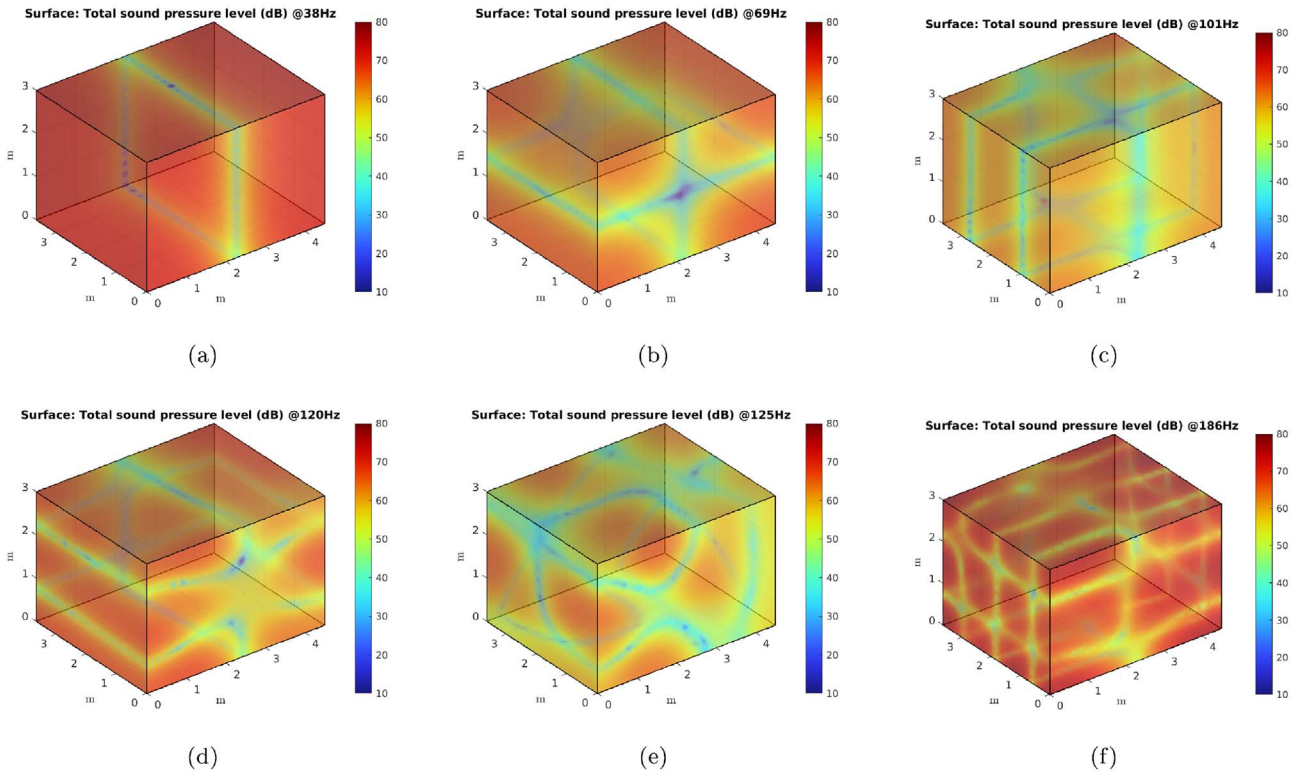


**Figure 10.** Total pressure distribution on the surfaces of the room without control at frequencies (a) 38 Hz, (b) 69 Hz, (c) 101 Hz, (d) 120 Hz, (e) 125 Hz, (f) 186 Hz.

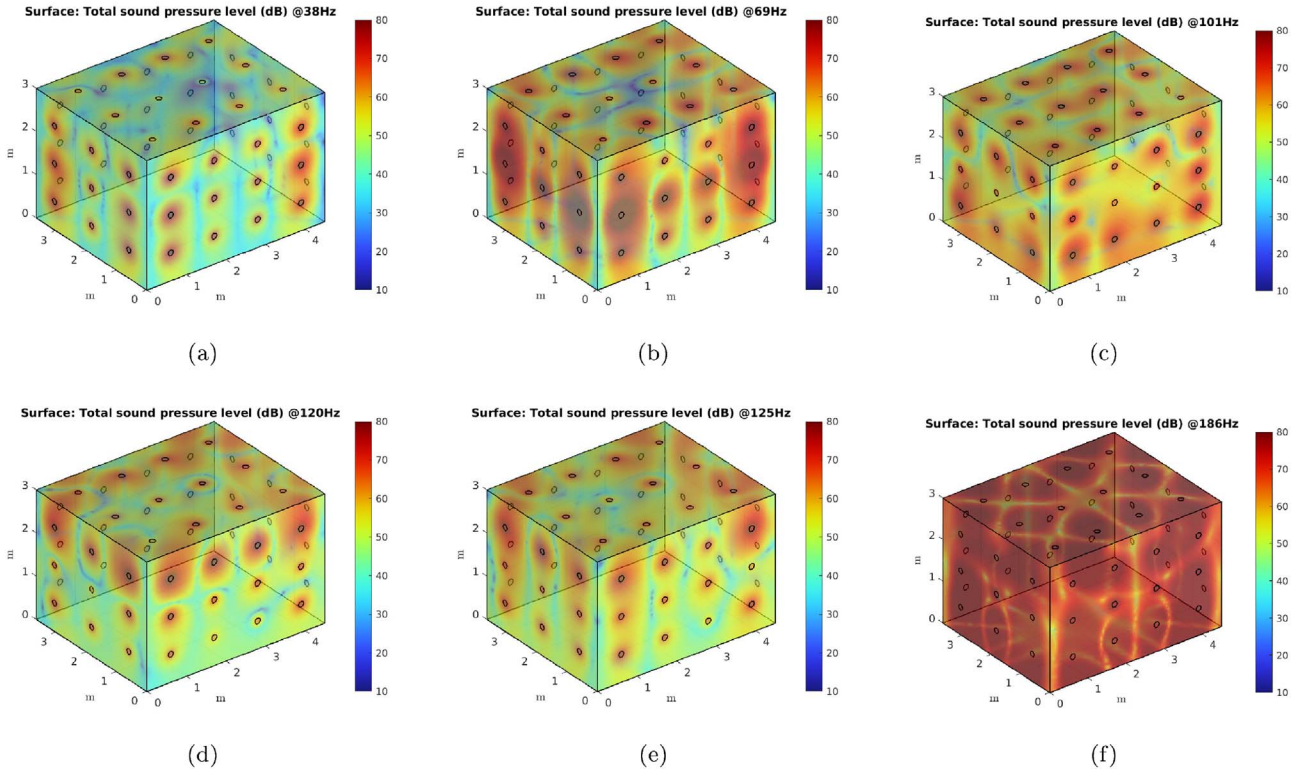


**Figure 11.** Total pressure distribution on the surfaces of the room with control at frequencies (a) 38 Hz, (b) 69 Hz, (c) 101 Hz, (d) 120 Hz, (e) 125 Hz, (f) 186 Hz.

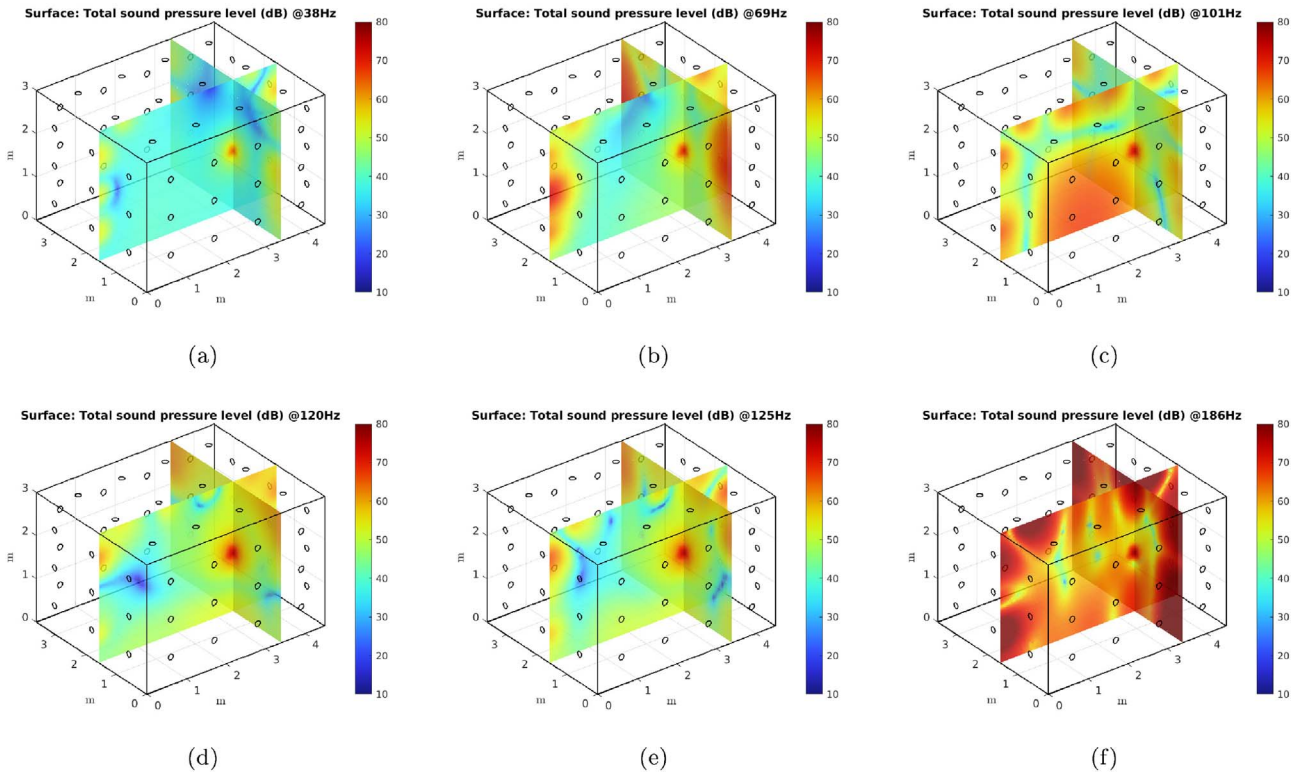


**Figure 12.** Total pressure distribution with control on transverse surfaces in the XZ and YZ planes of the primary source at (a) 38 Hz, (b) 69 Hz, (c) 101 Hz, (d) 120 Hz, (e) 125 Hz, (f) 186 Hz.

**Figure 13.** The demonstrator DADA.

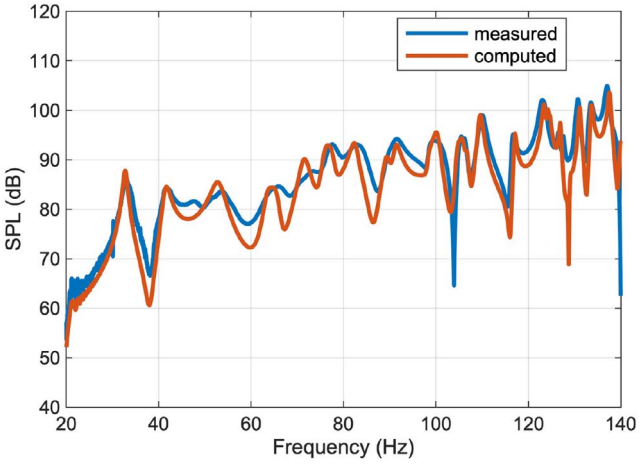


**Figure 14.** An source-microphone acoustic frequency response function in the demonstrator room.

control sources depends on the shape of the room modes to be controlled. This might be the basis of an optimization procedure to chose better locations for the transducers, perhaps allowing a more even control up to 180 Hz. This would however require a huge computation time and is beyond the scope of the present work.

## 5 Building of full-scale demonstrator

An experimental setup would be needed to validate the above simulations. This is however not a simple step, as such a demonstrator was not planned in the building. We could find a large enough free space potentially available for a long period, but not with the dimensions targeted nitially – which were used for the above simulations. We had therefore to change slightly the dimensions of the experimental setup, especially the intended ceiling height. Even if this might prove slightly less suited for an actual laboratory facility, it was considered as a good way to check many aspects of the principle of scattering control.

A test room was therefore built at the LMA to install and test the principle illustrated by Figure 1. This room, measuring 5.32 × 4.21 × 2.75 m, was made of double layered plasterboard (2 × 13 mm) lined with glass wool,

**Table 1.** Sound absorption coefficients for the demonstrator room.

| | 1/3 oct. band center frequency | | | |
|---|---|---|---|---|
| | 31.5 Hz | 63 Hz | 125 Hz | 250 Hz |
| Plasterboard (12 mm (1/2″) paneling on studs) | 0.29 | 0.29 | 0.29 | 0.1 |
| Door | 0.1 | 0.1 | 0.1 | 0.07 |
| Concrete (painted) | 0.01 | 0.01 | 0.01 | 0.01 |

standing on a thick concrete floor which is part of the building foundations. The only aperture is a double door made from solid wood with its frame fitted with seals. All surfaces were painted to improve insulation, leading to a very quiet facility with low absorption. When empty, it should therefore be very close to a rigid-walled rectangular room.

A truss structure has been installed, allowing to install control loudspeakers and microphones at almost arbitrary locations on the walls and the ceiling. They were at first positioned more or less randomly, following the guidelines resulting from 2D simulations. Figure 13 shows the demonstrator during transducers installation. The truss structure is also designed to support, in the future, panels of absorbent material.

A two-loudspeaker reference source, built at LMA, was used for a first acoustic characterisation of this demonstrator. It allows to estimate the instantaneous flow-rate from a pressure measurement inside the source. A dual-monopole model of this source has also been developed and validated through measurements in an anechoic room, allowing to estimate the direct field acoustic pressure at any location in the room [28].

For a first measurement, this source was located as close as possible to one room corner and a microphone (PCB model 376A32) was located at the opposite room. The distance between the source and microphone was 5.6 m. 20–400 Hz swept sines were sent to the reference source in order to obtain, following [29], the FRF between the source flow-rate and the microphone.

This initial measurement with no absorbent material has been used to update the 3D simulation model, both to take into account the actual dimensions of the room and to identify the unavoidable sources of absorption of the setup. Indeed, the measured FRF appeared to be quite different from the FRF computed using the 3D finite element model, including a uniform 2% wall absorption, used for the control simulations shown in the previous section. An update of the model parameters was therefore performed in order to provide a more representative model of the experimental facility.

Figure 14 compares the FRF obtained experimentally with the simulated one, over the 20 Hz to 140 Hz frequency range, with 0.125 Hz steps. The FEM model used the actual room dimensions and the absorption coefficients given in Table 1, estimated for a reasonable fit between the two curves. The associated wall impedances were taken as purely resistive for the computations. It was found that using separate absorption coefficients for a few frequency bands and for the door, walls and floor gave satisfactory results.

Figure 14 shows that the resonance and anti-resonance frequencies of the FRFs are in reasonable agreement as well as the responses levels. The absorption coefficients of the updated model are much higher than expected with plasterboard, particularly at very low frequencies. Vibration of the thin walls is probably a large source of absorption for low-frequency noise in the room. The finite element model however seems now suitable for optimising the configuration of the active scattering control setup.

## 6 Conclusion

The 2D semi-analytical model presented in Section 3 has shown that global control of the low-frequency wall reflections was possible with loudspeakers and microphones close to the walls. The miminisation signals accounting for the scattered pressure are obtained by linear filtering of the total pressure signals. The required filters can be identified from off-line measurements with a reference source whose free-field radiation is known. The 2D model is also a useful calculation tool for the preliminary design of a future installation.

The 3D FEM model presented in Section 4 allows a more accurate and realistic simulation of the room and the control sources. It confirms the efficiency of the control strategy. It will be useful for the fine tuning of the transducer locations, especially as it allows to detect potential misplacement of transducers, likely to prevent the efficient control of some specific modes. The complexity of the current software combination does however not allow an automatic process for the design of the setup.

An experimental room has been built at LMA for full-scale validation of the control strategy. Preliminary measurements using an existing reference source, allowed to characterise the room acoustics and to update the 3D finite element model. Indeed, an adjustment of the wall absorption was required to achieve realistic simulations. With this adjustment, the 3D finite element model produced calculated frequency response functions very similar to those measured in the actual room.

This work illustrated the interest of developing a digital twin of the planned facility – but also the difficulty to obtain a good match with the actual behaviour of the room, and the high CPU cost required for a realistic simulation. This emphasize the need to fully validate each step of the setup design before attempting the next one.

Ongoing work involves exhaustive measurements of the experimental setup without absorbing material fitted on the wall. Although not a realistic use of the room, this step

should allow to detect potential problems related to the building (i.e. parasitic sources of absorption) and to fine tune the 3D FEM model. This might result in a good match between responses, even at locations close to the walls. Control experiments, initially in open loop, will also be carried out in the near future after optimisation of the transducer positions using the 3D model.

A last step should be carried out after fitting absorbing material over the 5 walls, using the truss structure to leave a plenum behind a thin absorbing layer. This configuration, closer to the final realisation expected for an actual facility, should allow to assess the complementarity of the hybrid (passive/active) configuration over a wide frequency range. Much work is however needed, especially as it will probably require a more sophisticated 3D model.


## Acknowledgments

This work received support from the French government under the France 2030 investment plan, as part of the Initiative d'Excellence d'Aix-Marseille Université – A*MIDEX (AMX-19-IET-010).


## Conflicts of interest

Author declared no conflict of interests.

## Data availability statement

Data are available on request from the authors.

## References


1. IEC-60268-5: Sound system equipment – part 5: Loudspeakers, International Electrotechnical Commission, 2007.
2. ISO-3745: Acoustics – determination of sound power levels and sound energy levels of noise sources using sound pressure – precision methods for anechoic rooms and hemi-anechoic rooms, International Organization for Standardization, 2012.
3. ISO-9614-1: Acoustics – determination of sound power levels of noise sources using sound intensity – part 1: Measurement at discrete points, International Organization for Standardization, 1993.
4. ISO-9614-2: Acoustics – determination of sound power levels of noise sources using sound intensity – part 2: Measurement by scanning, International Organization for Standardization, 1996.
5. C.J. Struck, S.F. Temme: Simulated free field measurements, Journal of the Audio Engineering Society 42, 6 (1994) 467–482.
6. M. Melon, C. Langrenne, P. Herzog, A. Garcia: Evaluation of a method for the measurement of subwoofers in usual rooms, Journal of the Acoustical Society of America 127, 1 (2010) 256–263.
7. M. Sanalatii, P. Herzog, R. Guillermin, M. Melon, N. Poulain, J.-C. Le Roux: Estimation of loudspeaker frequency Response and directivity using the radiation-mode method, Journal of the Audio Engineering Society 67, 3 (2019) 101–115.
8. M. Sanalatii, P. Herzog, M. Melon, R. Guillermin, J.-C. Le Roux: Measuring the radiation of sound sources with the radiation mode method: towards realistic problems, Journal of the Acoustical Society of America 155, 3 (2024) 1641–1654.
9. E. Friot: Control of low-frequency wall reflections in an anechoic room, in: ACTIVE 2006, Adelaide, Australia, 18–20 September, Australian Acoustical Society, Australia, 2006, pp. CD–ROM (9 pages).
10. A. Gintz, E. Friot: Control of low-frequency wall reflections in an anechoic room: estimation of the scattered sound from wall measurements, in: 19th International Congress on Acoustics 2007, Madrid, Spain, 2–7 September, Sociedad Espanola de Acustica (SEA), 2007, pp. CD–ROM (5 pages).
11. C. Scandrett, Y. Shin, K. Hung, M. Khan, C. Lilian: Cancellation techniques in underwater scattering of acoustic signals, Journal of Sound and Vibration 272, 3–5 (2004) 513–537.
12. E. Friot, R. Guillermin, M. Winninger: Active control of scattered acoustic radiation: a real-time implementation for a three-dimensional object, Acta Acustica united with Acustica 92 (2006) 278–288.
13. Y.I. Bobrovnitskii: Impedance acoustic cloaking, New Journal of Physics 12, 4 (2010) 043049.
14. J. Cheer: Active control of scattered acoustic fields: cancellation, reproduction and cloaking, Journal of the Acoustical Society of America 140, 3 (2016) 1502–1512.
15. C. House, J. Cheer, S. Daley: An experimental investigation into active structural acoustic cloaking of a flexible cylinder, Applied Acoustics 170 (2020) 107436.
16. X. Cui, X. Wang, Z. Zhang, M. Wu, J. Yang: Active control of impulsive scattered sound based on virtual sensing, Applied Acoustics 214 (2023) 109678.
17. R. Haasjes, A.P. Berkhoff: An efficient offline scheme to compute an FIR controller for active reduction of acoustic reflections in an anechoic chamber, Journal of Sound and Vibration 573 (2024) 118198.
18. D. Habault, E. Friot, P. Herzog, C. Pinhède: Active control in an anechoic room: theory and first simulations, Acta Acustica united with Acustica 103, 3 (2017) 369–378.
19. E. Friot, A. Gintz: Estimation and global control of noise reflections, in: Active, Ottawa, CA, 23–26 August, 2009.
20. D. Habault, P. Herzog, E. Friot, C. Pinhède: ESAA project – toward an active anechoic room, in: 8th meeting of the GDRE, Greggynog, UK, 22–27 June, 2014.
21. P. Herzog, E. Friot, D. Habault, C. Pinhède, A. Gintz, P. Leroy, M. Pachebat, Toward an active anechoic room, in: Forum Acusticum, Krakow, Poland, 7–12 September, 2014.
22. C. Pinhède: Contrôle actif aux basses fréquences du champ diffracté en salle semi-anéchoïque, Ph.D. thesis, Aix-Marseille Université, 2019.
23. C. Pinhède, D. Habault, E. Friot, P. Herzog: Active control of the field scattered by the rigid wall of a semi-anechoic room – Simulations and full-scale off-line experiment, Journal of Sound and Vibration 506 (2021) 116134.
24. C. Pinhède, R. Boulandet, E. Friot, M.R. Allado, R. Côte, P. Herzog: Towards an active semi-anechoic room: simulations and first measurements, in: Forum Acusticum 2023, Torino, Italy, 11–15 September, European Acoustics Association, 2023. https://doi.org/10.61782/fa.2023.0399.
25. R. Boulandet, M. Allado, C. Pinhède, E. Friot, R. Côte, P. Herzog: Simulation of a hybrid (passive/active) acoustic measurement room, in: COMSOL 2023 Conference, Munich, Germany, 25–27 October, 2023.
26. N. Epain, E. Friot: Active control of sound inside a sphere via control of the acoustic pressure at the boundary surface, Journal of Sound and Vibration 299, 3 (2007) 587–604.
27. P.M. Morse, K.U. Ingard: Theoretical acoustics, Princeton University Press, Princeton, NJ, 1986.

28. C. Pinhède, P. Herzog: Design and measurement of a reference source at lower frequencies, in: Forum Acusticum, Lyon, France, 7–11 December, 2020, pp 3365–3372.

29. A. Novak, P. Lotton, L. Simon: Synchronized swept-sine: theory, application, and implementation, Journal of the Audio Engineering Society 63, 10 (2015) 786–798.

**Cite this article as**: Pinhède C. Boulandet R. Friot E. Allado MR. Côté R, et al. 2024. Towards an active semi-anechoic room: simulations and first measurements. Acta Acustica, **8**, 56. https://doi.org/10.1051/aacus/2024052.